Young Ossabaw Pigs Fed a Western Diet Exhibit Early Signs of Diabetic Retinopathy

Rayne R. Lim,[1–3] DeAna G. Grant,[4] T. Dylan Olver,[2] Jaume Padilla,[5–7] Alana M. Czajkowski,[8] Teagan R. Schnurbusch,[8] Rajiv R. Mohan,[1–3,9] Dean P. Hainsworth,[9] Eric M. Walters,[8] and Shyam S. Chaurasia[1–3]

[1]Ocular Immunology and Angiogenesis Lab, Department of Veterinary Medicine & Surgery, University of Missouri, Columbia, Missouri, United States
[2]Department of Biomedical Sciences, University of Missouri, Columbia, Missouri, United States
[3]Harry S. Truman Memorial Veteran Hospital, Columbia, Missouri, United States
[4]Electron Microscopy Core, University of Missouri, Columbia, Missouri, United States
[5]Department of Nutrition and Exercise Physiology, University of Missouri, Columbia, Missouri, United States
[6]Dalton Cardiovascular Research Center, University of Missouri, Columbia, Missouri, United States
[7]Child Health, University of Missouri, Columbia, Missouri, United States
[8]National Swine Resource and Research Center, University of Missouri, Columbia, Missouri, United States
[9]Mason Eye Institute, University of Missouri, Columbia, Missouri, United States

Correspondence: Shyam S. Chaurasia, Department of Veterinary Medicine and Surgery, College of Veterinary Medicine, University of Missouri, Vet Med Building, Room E115A, 1600 East Rollins Street, Columbia, MO 65211-5110, USA; chaurasias@missouri.edu.

Submitted: December 11, 2017
Accepted: April 9, 2018

Citation: Lim RR, Grant DG, Olver TD, et al. Young Ossabaw pigs fed a Western diet exhibit early signs of diabetic retinopathy. *Invest Ophthalmol Vis Sci*. 2018;59:2325–2338. https://doi.org/10.1167/iovs.17-23616

Purpose. Recent clinical data suggest an increasing prevalence of obesity and type 2 diabetes in adolescents, placing them at high risk of developing diabetic retinopathy during adult working years. The present study was designed to characterize the early retinal and microvascular alterations in young Ossabaw pigs fed a Western diet, described as a model of metabolic syndrome genetically predisposed to type 2 diabetes.

Methods. Four-month-old Ossabaw miniature pigs were divided into two groups, lean and diet-induced obesity. Obese pigs were fed a Western diet with high-fat/high-fructose corn syrup/high-choleric content for 10 weeks. Blood and retina were collected for biochemical profiling, trypsin digest, flatmounts, Fluoro-Jade C staining, electron microscopy, quantitative PCR, immunohistochemistry, and Western blots.

Results. Young Ossabaw pigs had elevated fasting blood glucose after feeding on a Western diet for 10 weeks. Their retina showed disrupted cellular architecture across neural layers, with numerous large vacuoles seen in cell bodies of the inner nuclear layer. Microvessels in the obese animals exhibited thickened basement membrane, along with pericyte ghosts and acellular capillaries. The pericyte to endothelial ratio decreased significantly. Retina flatmounts from obese pigs displayed reduced capillary density, numerous terminal capillary loops, and string vessels, which stained collagen IV but not isolectin IB4. Quantitative PCR and Western blots showed significantly high levels of basement membrane proteins collagen IV and fibronectin in obese pigs.

Conclusions. This is the first study to describe the ultrastructural neuronal and vascular changes in the retina of young Ossabaw pigs fed a Western diet, simulating early signs of diabetic retinopathy pathogenesis.

Keywords: diabetic retinopathy, Ossabaw pig, type 2 diabetes, microvasculature, basement membrane

Diabetic retinopathy (DR) is a progressive blinding disease characterized by the neuronal and microvasculature complications in patients with diabetes mellitus (DM). The International Diabetes Federation estimates there will be 629 million diabetics in the world by 2045,[1] of which 10% will be afflicted with some form of retinopathy within 10 years of the disease. DR in young adults is more commonly reported in patients with type 1 DM (T1DM). However, they form ~10% of the global DM pandemic.[1] The most alarming fact comes from the growing number of clinical reports that suggest the emerging trend of obesity and type 2 DM (T2DM) in adolescent children and young adults.[2–5] In fact, the full extent of T2DM prevalence in this young population on a global scale has not yet been reported. The Treatment Options for Type 2 Diabetes in Adolescents and Youth (TODAY) study group conducted one of the most extensive studies on adolescent T2DM in the United States and found ~14% incidence of retinopathy in their cohort.[6] Besides, the prevalence of DR is expected to magnify, especially in adolescents, as obesity and DM trend upwards due to the Western lifestyle that is characterized by physical inactivity and overnutrition.[4,7] Thus, a large population of young diabetic adults is at a risk of developing DR in their thirties to forties, resulting in a substantial economic burden.

Clinically, DR is broadly classified into early nonproliferative (NPDR) and late proliferative (PDR) stages. NPDR is asymptomatic; hence, early signs in NPDR are difficult, if not

impossible, to detect with modern advanced imaging techniques. One of the first evident signs of NPDR is retinal microaneurysms in DM patients.[8] However, recent understanding of DR indicates that diabetic retinal neurodegeneration precedes microvasculopathy.[9] Diabetic patients report subtle visual deficits shortly after diagnosis,[10,11] and postmortem examination of human DR retinas have revealed acellular capillaries, pericyte ghosts, and basement membrane (BM) thickening before the detection of microvascular changes.[12,13] Therapeutic and surgical interventions such as intravitreal anti-vascular endothelial growth factor (anti-VEGF) injection and laser photocoagulation are mostly administered during the PDR stage and can only delay the progression of DR pathogenesis. Currently, there are no clinical treatments available for NPDR patients as well as no neuro- and vasoprotective drugs available in the market to prevent early DR stages.

DR is a highly complex multifactorial disease that no single animal model can accurately represent.[14] Notably, human T2DM symptoms observed in the adolescent and young adults are difficult to replicate in rodents, as similar age and maturity are to be considered while studying disease pathology and progression. Commonly used T2DM models in DR studies include obesity-induced diabetic rodent models (db/db mice), Zucker diabetic fatty rats, and spontaneous T2DM models (Otsuka Long Evans Tokushima Fatty rat and Goto-Kakizaki rats). Zucker diabetic fatty rats and db/db mice are leptin receptor-deficient, making them obese without the underlying presentation of islet dysfunction or hyperglycemia seen in human patients.[15] Otsuka Long Evans Tokushima Fatty rats are severely obese and face criticism of irrelevance to human pathology due to their accelerated development of DR.[16,17] Goto-Kakizaki rats are the polygenic nonobese T2DM model that present few features of DR and, hence, are less widely used for retinal research.[17] Furthermore, the monogenic or polygenic mutations in rodent models do not represent the human etiology of diabetes.[16] Hence, large animal models such as pig might be more suited to study the progression of DR pathogenesis, with the added similarity of age, tissue size, and anatomy to that of diabetic human patients.

Ossabaw pigs are a breed of wild boar that adopted a "thrifty genotype" for survival under harsh conditions on the Ossabaw Island, Georgia, United States.[18] As a result, Ossabaw pigs are a model for diet-induced obesity and develop classic features of metabolic syndrome (MetS) when fed a high-fat diet.[19] Patients diagnosed with MetS are at higher risk of developing diabetes and cardiovascular diseases.[20,21] Young (6–9 months old) Ossabaw pigs representing the adolescent human age-group (14–18 years old) fed on a Western diet display features of MetS, along with hyperinsulinemia, glucose intolerance, hyperglycemia, and dyslipidemia.[19,22] The Ossabaw MetS model has been used for many diseases, including cardiovascular diseases,[23] steatohepatitis,[24] atherosclerotic lesions,[25] and renal injury.[26] However, the extent of retinal neuronal damage and microvasculopathy in the Ossabaw pigs are still unknown. This study investigated retinal, cellular, and vascular abnormalities in young Ossabaw pigs fed a Western diet.

Methods

Ossabaw Pigs

All experimental procedures were approved by the Institutional Animal Care and Use Committee, University of Missouri Columbia and adhered to the ARVO Statement for the Use of Animals in Ophthalmic and Vision Research. Adolescent female and male Ossabaw mini pigs (RRID:NSRRC:0008) were housed at the Animal Science Research Center, University of Missouri, Columbia, Missouri, United States, in a temperature-controlled environment with a 12-hour light and dark cycle. Following weaning, all pigs were fed a standard commercially available chow diet (catalog no. 5L80, Lab Diet; 3.03 kcal/g, 71% from carbohydrate, 18.5% from protein, and 10.5% from fat) until 3.5 months of age. Twelve pigs were then divided into lean (n = 6; 4 female/2 male) and obese (n = 6; 3 female/3 male) groups. Lean pigs were kept on the standard chow, while pigs in the obese group were fed a high-fat/high-fructose corn syrup/high-calorie diet (5B4L, Lab Diet; 4.14 kcal/g, 40.8% from carbohydrate, 16.2% from protein, and 43% from fat) for 10 weeks. At six months of age, following a 20-hour overnight fast, pigs were anesthetized (5 mg/kg of Telazol and 2.25 mg/kg of xylazine mixture) and weighed (for body mass determination), blood samples were collected from the jugular vein, and pigs were subsequently euthanized for tissue collection. Plasma was analyzed for lipids, insulin, and glucose profiling (CPath LLC, Columbia, MO, USA).

Porcine Eye Collection and Retina Dissection

Following euthanasia, eyelids were removed using blunt scissors for easier access to the eye globe. Curved iris scissors were used to sever the ocular muscles, connective tissues, and nerves around the globe. Twelve globes were collected from each group, with n = 3 eyes each taken for electron microscopy (EM), trypsin digest, flatmount immunostaining, immunohistochemistry, real-time PCR, and Western blot. To isolate retinal tissue, the pig eye was placed on ice, in a petri dish with cold, sterile PBS. An incision was made at the ora ciliaris, approximately 5 mm posterior to the corneal limbus, by using a #11 scalpel blade. A circumferential cut was made to remove the anterior ocular tissues, including the ciliary body and lens. The vitreous body was removed carefully without detaching the retina, the eyecup was submerged immediately in cold, sterile PBS, and the retina was peeled off the underlying choroid under a Leica S6 E stereomicroscope (Leica Microsystems Inc., Buffalo Grove, IL, USA). The retinal tissue was processed immediately for biochemical analysis.

Electron Microscopy

The cornea and lens were removed as described above, and the vitreous body was left intact to prevent disruption to the retina. One milliliter of EM primary fixative (2% paraformaldehyde, 2% glutaraldehyde in 100 mM sodium cacodylate buffer; pH 7.35) was injected into the vitreous cavity of the eye to fix the retina by using a 1-cc syringe and a 25-gauge needle. To avoid torque on the vitreous body, the needle was removed and repositioned between each injection of fluid to reach all parts of the retina. The eyecup was then submerged in the fixative and kept at 4°C for 24 hours. For subsequent EM processing, selected retinal areas temporal to the optic nerve were segmented into 3-mm retinal cubes. Each cube was immobilized in HistoGel (Thermo Fisher Scientific, Waltham, MA, USA) and rinsed with 100 mM sodium cacodylate buffer (pH 7.35) containing 130 mM sucrose. A solution of 1% osmium tetroxide in cacodylate buffer was used for secondary fixation. After an hour at 4°C, each cube was subjected to en bloc staining using 1% aqueous uranyl acetate. Following overnight incubation at 4°C, graded dehydration series (100 watts for 40 seconds per exchange) was performed using ethanol. Tissues were then transitioned into acetone and infiltrated with Epon resin (250 watt for 3 minutes) and polymerized at 60°C overnight. Retinal cubes were cut transversely with an ultramicrotome to obtain 2-μm thick sections for histologic examination. Each retina tissue block was further trimmed to a length of 500μm and cut with a diamond knife to yield 75-nm sections for transmission

EM. Images were acquired with a JEOL JEM 1400 transmission electron microscope (JEOL USA Inc., Peabody, MA, USA) at 80 kV on a Gatan Ultrascan 1000 CCD, at 1200× magnification.

BM Measurements

Retinal capillaries with visible BM and endothelial/pericyte boundaries were imaged under the electron microscope for measurement of BM thickness, as previously described.[27–29] Only capillaries with vessel area between 10 and 30 μm^2 were taken for the analysis. At least 10 capillaries were taken from each layer of the capillary plexus for each eye. Each retinal capillary was overlaid with 20 radiating lines, each 18° apart to form the wheel of a 20-spoke radial grid, with the center of the grid placed at the center of the vessel. Widths of the BM at each point of intersection were measured using ImageJ software (ImageJ, National Institutes of Health, Bethesda, MD, USA), by drawing a straight line perpendicular to the boundaries of the BM. Measurements from all spokes were averaged to obtain BM thickness for each capillary. Analysis of retinal capillaries was done in a masked manner.

Toluidine Blue Staining and Capillary Density Quantification

Retinal sections of 2-μm thickness from EM cubes were stained with toluidine blue for 1 minute, washed with distilled water, and dried on a slide warmer. Light microscopy images were taken across the length of the retina by using the Leica DM4000 (Leica Microsystems Inc.) at 400× magnification. For quantification of capillary density, the number of capillaries seen with an open lumen in the inner plexiform layer were counted and divided by the total surface area (mm^2) of the retina in the microgram. Three retina blocks from different areas of the eye were processed for histology, and $n = 3$ sections were collected intermittently at different depths from each block for quantification.

Trypsin Digest

Due to the similarities between pig and human retina, retinal trypsin digest was performed according to the method described by Boeri et al.,[30] with slight modifications. Briefly, the cornea, lens, and ciliary body were removed as described above. With the vitreous intact, 10% neutral buffered formalin was injected into the vitreous cavity of the eye and submerged in fresh 10% neutral buffered formalin at room temperature. After 72 hours, the eye was removed from the fixative, halved at the midsagittal plane, and placed in 0.15 M glycine (in 50:50 H_2O to PBS) at 4°C. The glycine solution was changed three times before leaving eyes overnight. Eye halves were removed and placed in a petri dish with filtered distilled H_2O. Each half was cut radially to size, and the retina was carefully peeled off the choroid. Isolated retinal pieces were placed in a 6-well plate and incubated with 3% trypsin 1:250 (Amresco, Solon, OH, USA) in a 0.1 M Tris solution (pH 7.4) for 1.5 hours in a shaking incubator at 37°C. The trypsin solution was replaced with filtered distilled water, and the retina was allowed to shake overnight at room temperature. The vitreous was removed from the retina by pulling it off with blunt forceps. The retina was subjected to a second trypsin incubation for 2 hours at 37°C, then washed overnight with filtered distilled water. Adherent cells were removed from the retinal vasculature by using gentle agitation. The vasculature was then transferred to a glass slide by using a glass pipette and left to dry completely on the bench. After the vessels turned white, Periodic acid Schiff staining (Abcam, Cambridge, MA, USA) was performed according to manufacturer's instructions. Slides were dehydrated in graded ethanol and xylene and mounted with Vectamount (Vector Laboratories, Burlingame, CA, USA). The retinal vasculature was visualized under a Leica DM4000 light microscope (Leica Microsystems Inc.).

Pericyte Loss and Acellular Capillaries

To quantify pericyte loss and acellular capillaries in the pig retina, at least 10 images of the retinal trypsin digest were taken at 400× magnification for each animal. The total number of pericyte cells, endothelial cells, and acellular capillaries, and the total length of capillaries in each image were counted by a masked observer by using ImageJ software. Pericyte loss was determined by taking the ratio of total pericyte cells counted per total endothelial cells counted in the lean and obese pigs. Retinal pericyte distribution in the retina was represented by total pericyte cells per 400× magnification field in each group. Acellular capillaries were presented as the total number of acellular capillaries counted per millimeter length of the capillary.

Retinal Flatmounts

The pig eye was dissected as described above to remove the anterior ocular tissues and vitreous body. The eyecup was submerged immediately in 4% paraformaldehyde for 30 minutes on ice, then cut into 4 to 8 pieces in a radial manner by using sharp scissors. The retina was carefully peeled from the underlying choroid by using blunt forceps. Intact retinal pieces were placed in a 12-well plate for ease of use on a shaker during flatmount staining. The retina was first washed twice with PBS for 5 minutes each. Blocking was done using 0.2% BSA with 5% donkey serum in 0.3% Triton X-100 in PBS (PBST) for 2 hours at room temperature. Collagen IV (1:100; Abcam) was diluted in blocking buffer and allowed to stain overnight at 4°C. After washing thrice, secondary antibody (1:500; Life Technologies, Carlsbad, CA, USA) was added with Isolectin GS-IB4 (1:100; Life Technologies) in 0.2% BSA (in PBST) and left overnight. Following the washing steps, the retina was counterstained with Hoechst (1:2000; Life Technologies) for 10 minutes and mounted with Prolong Diamond (Life Technologies). Staining was visualized using a Leica DM4000 microscope under fluorescence excitation.

Immunohistochemistry

Twelve-micron-thick retinal sections were collected, postfixed with ice-cold acetone for 10 minutes, and blocked with 5% donkey serum for 1 hour at room temperature. Immunostaining was performed using collagen IV (1:100; Abcam) and fibronectin (1:50; BD Biosciences, San Jose, CA, USA) kept overnight in 4°C, and secondary stained with Alexa-Fluor 594 antibody (1:500; Life Technologies) for 1 hour. The retina was mounted using Vectashield with 4′,6-diamidino-2-phenylindole (DAPI; Vector Laboratories) and visualized using a Leica DM4000 fluorescence microscope.

Fluoro-Jade C (FJC) staining

FJC staining (MilliporeSigma, Burlington, MA, USA) was performed on 20-μm thick retinal sections according to manufacturer's instructions, with slight modifications. Briefly, sections were immersed in a basic alcohol solution (1% NaOH in 80% EtOH) for 5 minutes, followed by 2 minute rinses in 70% EtOH and distilled water each. Blocking was performed with a 10-minute incubation in 0.06% potassium permanganate solution, followed by a 2-minute rinse in distilled water. A FJC working solution (0.001%) containing Hoechst (Life Technol-

Investigative Ophthalmology & Visual Science

ogies) was placed onto retinal sections and incubated at room temperature for 10 minutes. Slides were washed three times in distilled water and dried at 50°C on a slide warmer. Xylene was used before mounting in DPX nonfluorescent mounting media (MilliporeSigma). Staining was visualized using a Leica DM4000 fluorescence microscope.

Real-Time PCR (qPCR)

Retinal tissues were homogenized in 350 µL of RLT buffer (Qiagen, Valencia, CA, USA) by using a motor pestle. RNA was isolated using the RNeasy Mini Kit (Qiagen) according to the manufacturer's instructions. Reverse transcription was performed using GoScript (Promega, Madison, WI, USA), with 500 ng of RNA for every 20-µL reaction. qPCR was performed on the ViiA7 (Applied Biosystems, Foster City, CA, USA) with PowerUp SYBR green dye (Thermo Fisher Scientific) by using the following primers: pig collagen IV (forward, 5′-GCGAAGA GGAAAAGTCGTG-3′; reverse, 5′-ATCAACACCTTTGGGACCC G-3′), pig fibronectin (forward, 5′-CAGCTCCGAGATCAGTGCA T-3′; reverse, 5′-TCCGAATCCTGGCATTGGTC-3′), pig β-actin (forward, 5′-AGATCAAGATCATCGCGCCT-3′; reverse, 5′-AT GCAACTAACAGTCCGCCT-3′). The cycle profile included a preincubation step for 2 minutes at 50°C, then 2 minutes at 95°C, and 45 amplification cycles at 95°C for 15 seconds and 60°C for 1 minute.

Western Blot

Frozen retinal tissues were weighed, and 30 mg from each eye was homogenized in 300 µL radioimmunopreciptation assay buffer (Cell Signaling Technology, Danvers, MA, USA) by using the motor pestle. Protein estimation was performed using the bicinchoninic acid assay (Pierce Biotechnology, Rockford, IL, USA). A total of 50 µg of protein lysate was run on an 8% Tris-Glycine gel (Life Technologies) under denaturing conditions. Proteins were transferred onto a nitrocellulose membrane (Li-Cor, Lincoln, NE, USA) by using the semidry method. Immunoblotting for collagen IV (1:200; MilliporeSigma) and fibronectin (1:500; BD Biosciences) was performed according to the standardized protocol. In brief, 5% milk was used as blocking agent and antibody diluents. Blots were shaken with the antibodies overnight at 4°C, and horseradish peroxidase-conjugated secondary antibody incubation was performed at room temperature for 1 hour. Protein immunoreactive bands were visualized using SuperSignal substrates (Pierce Biotechnology) and detected using a C-Digit imaging system (Li-Cor). Densitometry was calculated using the Li-Cor Image Studio software, and all blots were normalized to the β-actin housekeeping protein.

Statistical Analysis

Statistical analysis was performed using the Student's *t*-test (GraphPad Prism 6.0; GraphPad Software, Inc., La Jolla, CA, USA) for comparison between lean and obese groups. Significance was taken when $P < 0.05$. Data were presented as mean ± SD.

Results

Ossabaw Pigs on Western Diet Show Signs of T2DM

Relative to lean control pigs, obese pigs had a ~40% increase in body mass (Fig. 1A) after 10 weeks on the Western diet. Obese pigs displayed increased plasma glucose (Fig. 1B) and insulin (Fig. 1C) concentrations. The Homeostatic Model Assessment of Insulin Resistance (HOMA-IR), a clinical indicator of insulin resistance, was also elevated in obese Ossabaw pigs (Fig. 1D). In humans, HOMA-IR values >1.9 are considered indicative of insulin resistance. Due to the composition of the diet, there is also an expected significant increase in high-density lipoprotein (HDL) (Fig. 1F), low-density lipoprotein (LDL) (Fig. 1G), and plasma cholesterol (Fig. 1H) in the obese group. However, the elevated level of triglyceride (Fig. 1E) in the obese animals was not significant.

Obese Ossabaw Pig Retinas Exhibit Ultrastructural Neural Degenerative Changes

Histologic and EM examination (Figs. 2, 3) of the obese Ossabaw pigs showed changes in the neuronal architecture in almost every layer of the retina, without any loss of thickness. The distribution of cellular and plexiform layers was maintained, but cellular derangement and less compaction were observed in the obese Ossabaw pigs. The retinal pigmented epithelium (RPE) in both groups was in good contact with the photoreceptor (PhR) outer segment discs, showing no signs of detachment during processing. The obese pigs appeared to have a reduction in the number of photopigments in the apical side of the RPE (Fig. 2B). However, this could be a result of oblique sectioning. Nonetheless, RPE nuclear distortion was observed under EM examination (Fig. 3B, white arrow). The PhRs in both groups were largely well organized, with no discernible differences in shape or distribution (Fig. 2), except implosion in the PhR inner segment (Fig. 3D, white arrowhead), disarrangement in cone discs (Fig. 3D, black arrow), and smaller cone ellipsoid (Fig. 3F) were seen in the obese pigs. The outer limiting membrane appeared to be intact and continuous throughout the lean and obese retinas (Figs. 3G, 3H). The outer nuclear layers of the PhR cell bodies were less organized in the obese pigs (Fig. 2B), with increased gaps between the PhR nuclei, which were of uneven sizes and shapes (Fig. 3J) as compared to the lean control (Fig. 3I). Atrophic PhR nuclei were also seen in the obese pigs (Fig. 3J, black arrowhead). The inner nuclear layer (INL) showed disorganization of cells in the obese pigs, with uneven distribution of nuclear/cytoplasmic content. One of the most abundant cells in the INL is the horizontal cells,[31] which were markedly shrunken in the obese pigs (Fig. 2B). Furthermore, large vacuoles were also seen throughout the INL cells (Fig. 3N, black asterisk). No discernible differences were seen in the inner plexiform layer (IPL) of both groups (Figs. 3O, 3P). The ganglion cells in the ganglion cell layer (GCL) were visible and easy to identify in lean control animals (Figs. 2A, 3Q); however, numerous densely stained disintegrated cell bodies were seen in the GCL of the obese animals (Figs. 2B, 3R, white asterisk). There was no disruption in the nerve fiber layer of the obese versus lean control, although the neuronal processes appeared swollen (Fig. 3T, thick white arrow) in the former.

FJC staining was performed to support the cell morphologic abnormalities seen in the obese Ossabaw pig retinas. FJC stains the cell bodies and dendritic tree of degenerating neurons in the retina.[32] Few cells were seen stained in the inner retina of the lean Ossabaw pigs (Fig. 2C, arrowheads), presumably in the astrocytes at the GCL and capillaries in the IPL and INL. Strong staining was observed in the obese Ossabaw pigs across all layers of the retina, indicative of degenerating cells (Fig. 2D, arrowheads).

BM Thickening and Increased Expression of Basal Lamina Components

BM thickening is one of the histologic hallmarks of the early stages of DR pathogenesis. To quantify this in the pigs, capillaries in the retina were imaged for BM analysis by using

Investigative Ophthalmology & Visual Science

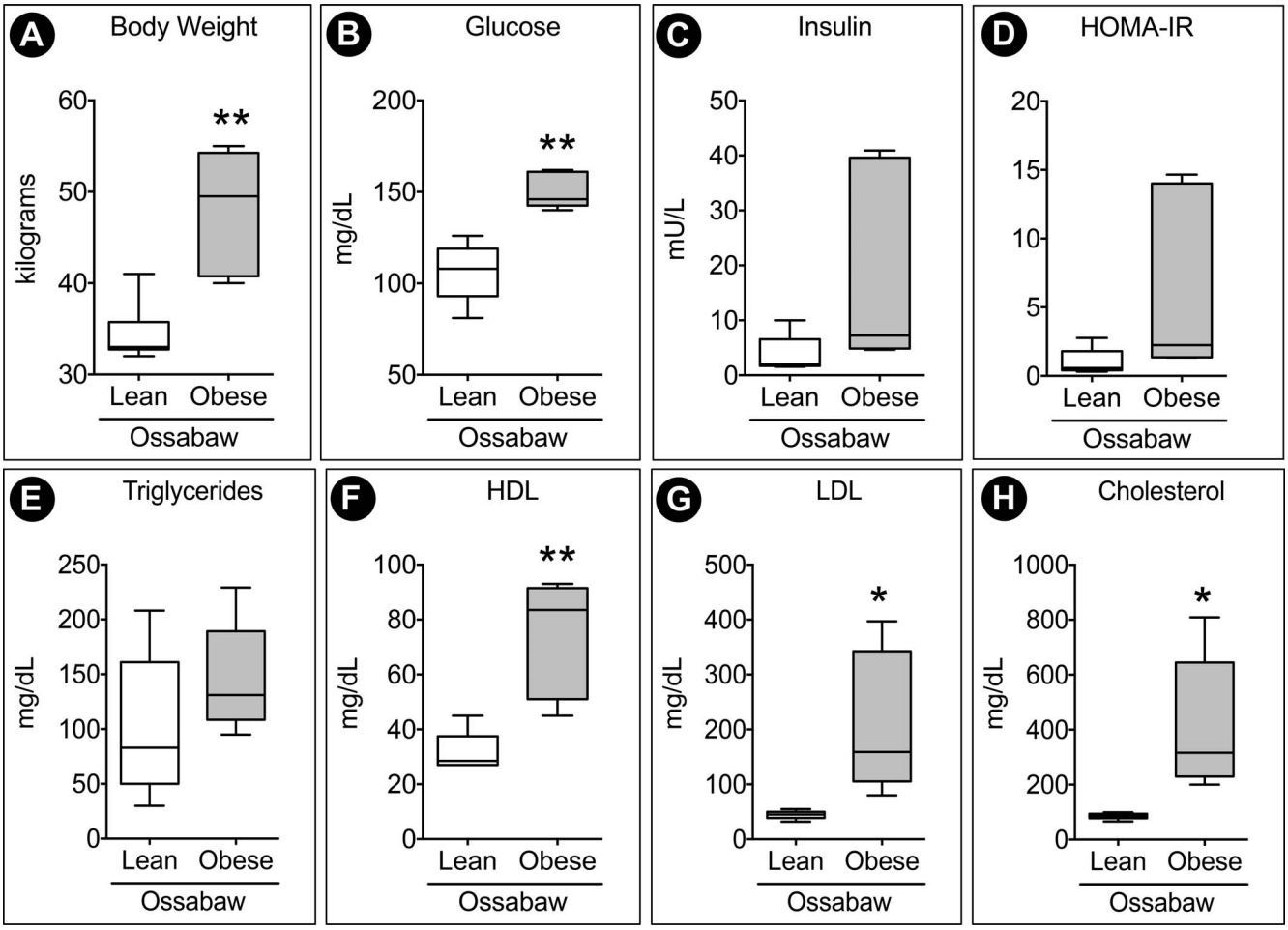

Figure 1. Ossabaw pigs fed a Western diet exhibit signs of hyperglycemia and hyperlipidemia. (**A**) Pigs showed ~40% weight increase following 10 weeks of the Western diet. Blood profiling of 20-hour fasted pigs showed an increased trend of (**B**) plasma glucose and (**C**) plasma insulin. (**D**) HOMA-IR, calculated by insulin (mU/L) × glucose (mg/dL), was elevated, indicating insulin resistance in obese pigs. (**E–H**) Hyperlipidemia was characterized by an increase in HDL, LDL, and cholesterol. $n = 6$ animals per group. $^{*}P < 0.05$ and $^{**}P < 0.01$.

the 20-spoke method. Because pigs have a trilaminar vascular system similar to humans,[31] the superficial plexus at the GCL, intermediate plexus at the IPL, and deep plexus at the INL/outer plexiform layer (OPL) were analyzed separately. A 20-spoke wheel was overlaid across each EM image, and the shortest perpendicular distance between the BM boundaries (Fig. 4, arrowhead) at each spoke intersection was measured. Obese pigs had an increased BM thickness at the GCL (Fig. 4A), IPL (Fig. 4B), and INL/OPL (Fig. 4C) capillary plexi, with significant thickening especially in the IPL and INL/OPL. The overall increase was supported by qPCR and Western blot analysis of the major components of the retinal capillary BM scaffold. Obese pigs showed higher transcript levels of fibronectin and collagen IV (Fig. 5A) and elevated protein expression (Fig. 5B). In addition, immunohistochemistry for the BM proteins showed increased staining of fibronectin (Fig. 5C) and collagen IV (Fig. 5D) in the obese Ossabaw pig retinal capillaries.

Ossabaw Pigs Fed a Western Diet Depict Acellular Capillaries, Pericyte Ghost, and Cell Loss

Because the earliest structural damage observed in the pathogenesis of DR is pericyte loss and acellular capillaries, trypsin digest was employed to examine the Ossabaw retinal vasculature. Lean Ossabaw pig retinas had capillaries of even caliber widths (Fig. 6A), with an endothelial cell (arrow) usually accompanied by a darker stained pericyte cell (black arrowhead). Obese Ossabaw retinal capillaries had different calibers, as seen in Fig. 6A, with numerous pericyte ghosts (Fig. 6B, white arrowhead) and pericyte dropouts (Fig. 6C, black arrowhead). Cell counts of at least 10 retinal fields in each animal estimated the pericyte to endothelial cell ratio to be 0.5, indicating one pericyte cell for every two endothelial cells (Fig. 6E). This ratio was decreased in the obese Ossabaw pigs ($P < 0.001$). This significant reduction in the number of pericytes ($P < 0.001$) available to support capillaries in the obese pig retinas (Fig. 6F) led to the increased number of acellular capillaries formed (Fig. 6I). Migratory pericytes seen in both lean and obese groups had a triangular nucleus and bridge two capillaries by threadlike extensions (Fig. 6A, asterisk). These threadlike vessels with or without nuclei were not counted as acellular capillaries in this study. Instead, vessels with a thicker vessel devoid of nuclei were quantified (Figs. 6F, 6H, thick arrow).

Western Diet Resulted in Arteriolar Narrowing and Reduced Capillary Density in Ossabaw Pigs

To further study the retinal vascular architecture, we performed isolectin IB4 and collagen IV double immunostaining on retinal flatmounts to examine the damage to the endothe-

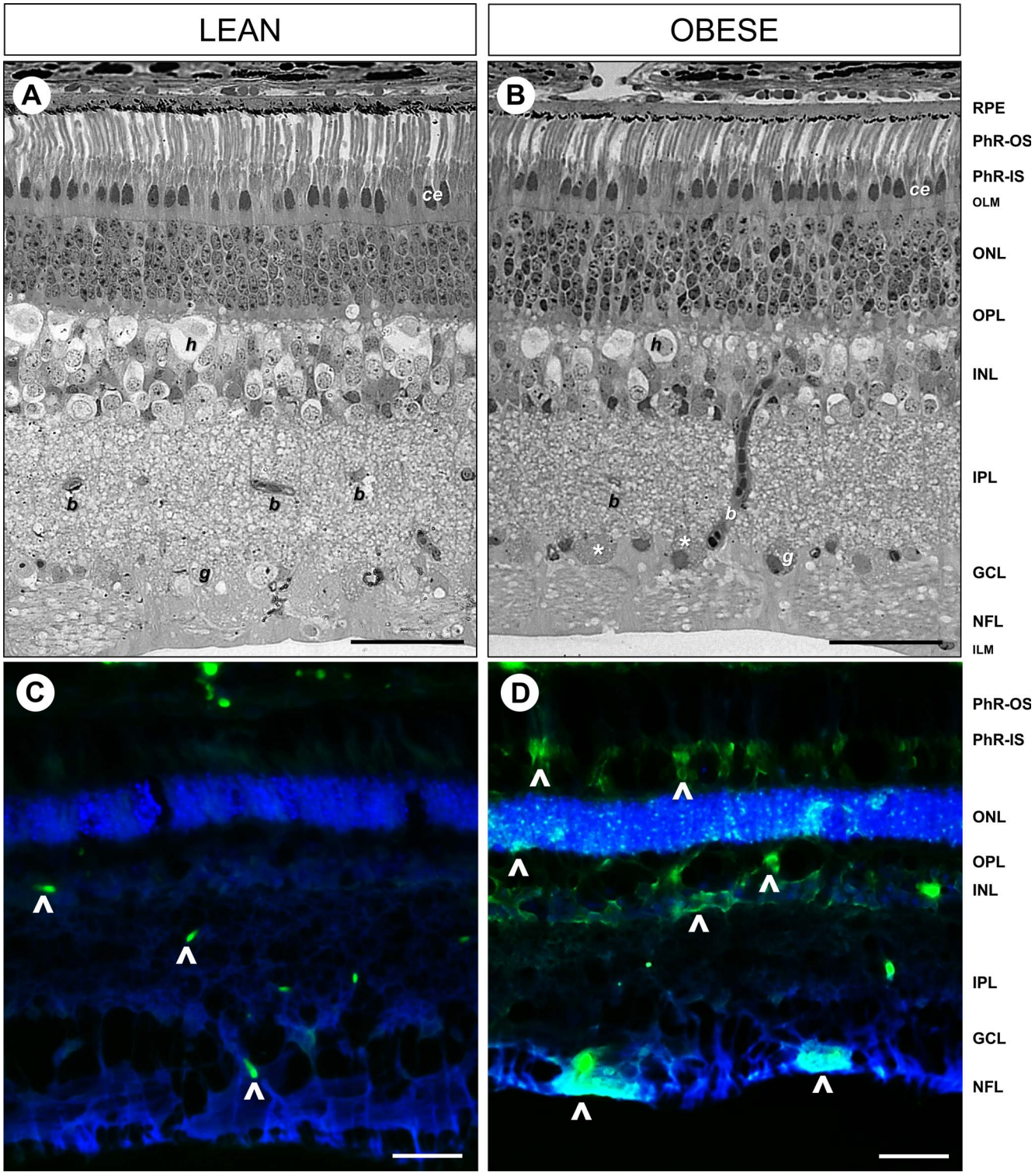

Figure 2. Cellular derangement of retinal structure and degenerating neurons in the Western diet-fed Ossabaw pigs. Light microscopy of toluidine blue staining on 2-μm thick resin-embedded retinal sections revealed intact and organized cellular structures in (**A**) lean control pigs, which were disrupted in the (**B**) obese Ossabaw pigs. FJC staining to visualize degenerating neurons (*arrowheads*) in (**C**) lean and (**D**) obese Ossabaw pigs showed increased labeling of cell bodies in the nerve fiber layer (NFL), INL, and PhR of the obese animals. PhR-IS, photoreceptor inner segment; OLM, outer limiting membrane; ONL, outer nuclear layer; OPL, outer plexiform layer; ILM, inner-limiting membrane; *g*, ganglion cell; *b*, blood vessel; *h*, horizontal cell; *ce*, cone ellipsoid. $n = 3$ eyes per group. *Scale bar*: 50 μm.

lial/mural cells and BM, respectively. Obese Ossabaw pigs showed an overall reduction in microvasculature density and branching from the arterioles (Figs. 7A, 7B). Disruption to the capillary network was more apparent in the intermediate and deep plexi (Figs. 7C, 7D). This was similarly observed in the retinal histology, where numerous blood vessels were seen in the IPL of the lean pigs (Fig. 2A, *b*), which was reduced in the obese group (Fig. 2B). The possibility of different sectioning

Investigative Ophthalmology & Visual Science

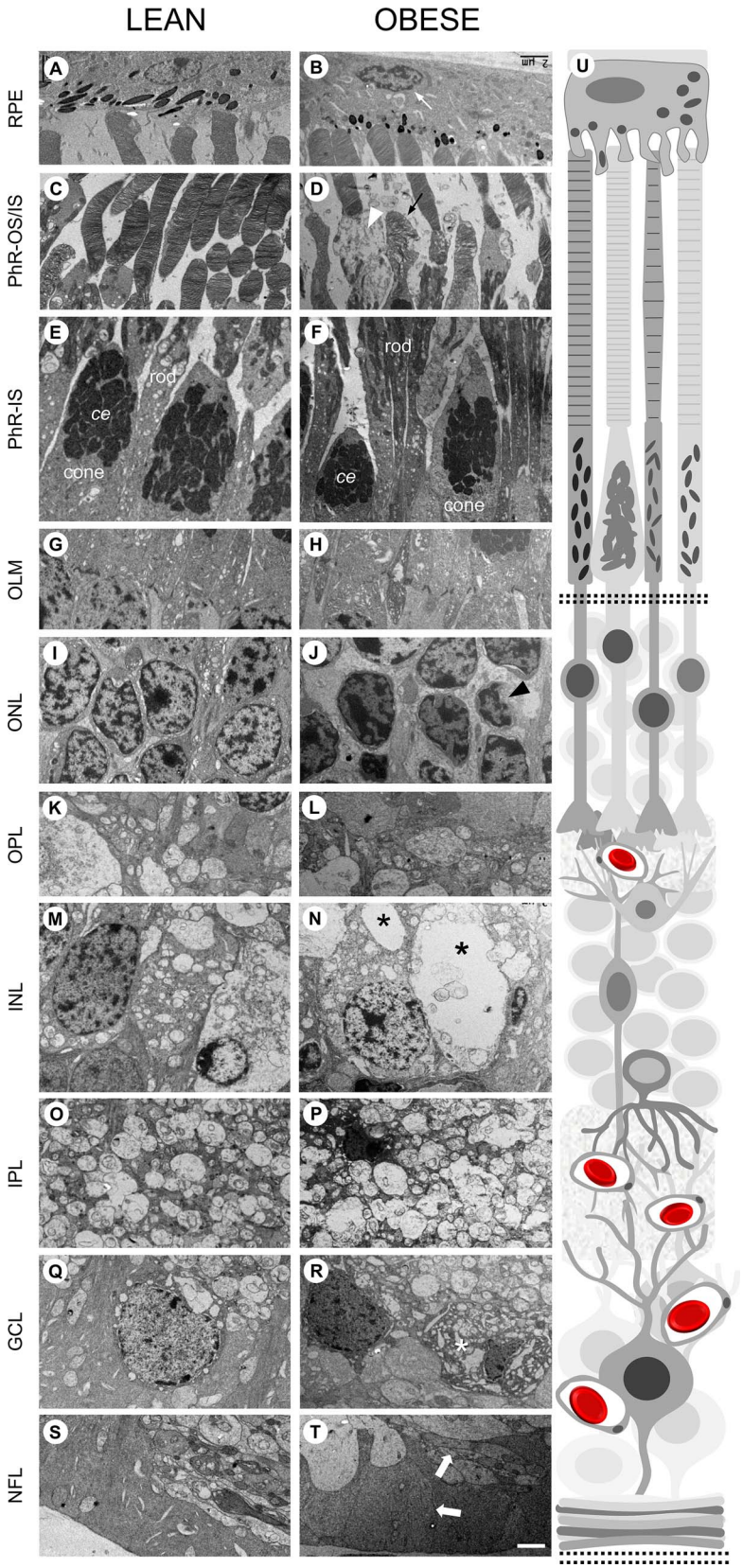

Figure 3. Obese Ossabaw pig retina displays multiple neuronal and cellular defects. Representative EM images for all layers of the retina, with (**U**) schematic of retina structure on the right. (**A**, **B**) RPE was intact in both lean and obese pigs. However, nuclear atrophy (*white arrow*) was seen in the latter. (**C**, **D**) PhR outer segment cone disc (*black arrow*) and PhR inner segment (*white arrowhead*) were seen to be disrupted in obese Ossabaw pig. (**E**, **F**) Smaller cone ellipsoid (*ce*) was seen in the PhR inner segment of the obese pig. (**G**, **H**) The outer limiting membrane was intact and continuous in both groups of animals. (**I**, **J**) The outer nuclear layer in Western diet-fed pigs had increased gaps between PhR nuclei and signs of

Investigative Ophthalmology & Visual Science

atrophic nuclei (*black arrowhead*). (**K**, **L**) The OPL in both groups of pigs did not show discernible differences. (**M**, **N**) The INL in obese pigs were marked by hypervacuolations (*black asterisk*) in numerous neuronal cell bodies. (**O**, **P**) The IPL in both groups of pigs did not show discernible differences. (**Q**, **R**) The GCL in Western diet-fed pigs showed numerous densely stained disintegrated cell bodies (*white asterisk*). (**S**, **T**) The nerve fiber layer had indications of axonal swelling (*block arrow*) in the obese Ossabaw pigs. $n = 3$ eyes per group. *Scale bar*: 2 μm.

angles or selection of retinal areas were ruled out, as the PhR in both groups showed similar profiles, and retina cubes in similar regions of the retina were chosen for analysis. A bridging vessel commonly seen travelling from the superficial to deep capillary plexi in the pig retinas is represented in Fig. 2B. Quantification of the IPL capillary count per retina cross section area (Table) revealed a significant decrease in capillary density in the obese pigs ($P < 0.01$). In addition, numerous terminal capillary tubes were seen in the obese animals (Fig. 7E), which were absent in the lean controls. These microvasculature damages are indicative of the early retinopathy often seen in postmortem human retinas. Double staining of isolectin IB4 and collagen IV allow for the identification of acellular capillaries, which are empty tubes of BM, positive for collagen IV but negative for IB4. Fig. 7F shows the representative image of an acellular capillary seen in the obese Ossabaw pigs.

Discussion

Recent clinical data suggest that the age of diabetes onset could contribute to the aggravation of DR progression in youths. T2DM is usually not seen in prepubertal adolescents,[33] but the risk of developing DR in adolescents with T2DM after puberty is 4.8-fold higher[34] and reportedly faster in these youths.[35] The World Health Organization defines the human adolescent to be aged between 10 and 19 years, corresponding to the first year in a pig's life, because these animals do not follow a linear age progression as that of humans. Sows and boars are sexually mature by 5 to 6 months of age.[36] Therefore, 6-month-old Ossabaw pigs were selected for this study to mimic preexisting obesity in adolescents before the diagnosis of T2DM. This allowed us to accurately map the time-course development of DR pathogenesis in the early stages of obesity-induced DM and dyslipidemia, which will eventually lead to detectable DR.

T2DM is often accompanied by obesity and dyslipidemia. The majority of the adolescents who developed T2DM were reported to be obese.[5,37] A recent report suggests that DR among young T2DM patients is more prevalent than described in the literature.[38] Thus, Viner et. al.[2] presented a persuasive case for the need to classify adolescent T2DM as a "severe progressive phenotype," due to their tendency for not being diagnosed, which causes the high risk of developing complications within affected children and young adults. This could be attributed to the delayed detection of T2DM in youths, underestimation of duration between DM diagnosis and DR detection, and lack of ophthalmic screening postdiagnosis.[38] Moreover, little is known about retinopathy progression in adolescent/young T2DM patients due to the unavailability of a suitable animal model to mimic the early-onset of DR to understand disease pathogenesis. Of the many available T2DM animal models mentioned in the literature where the DR phenotype was studied, none of them represent retinopathy in juvenile/adolescent/young patients with T2DM.[14] The Ossabaw pig fed a high-fat diet has been described as a model for MetS and has been extensively studied for cardiovascular and metabolic disorders.[19,21,22,25] However, retinal changes in young Ossabaw MetS pigs have not yet been reported. This is the first study to investigate the cellular and vascular abnormalities in the retina of young Ossabaw pigs fed a Western diet of high-fat/high-fructose corn syrup/high-calorie content for 10 weeks. These obese pigs showed systemic signs of hyperglycemia, hyperinsulinemia, and dyslipidemia. They exhibited characteristic features of early stages of DR, including cellular derangement, neurodegenerative changes, pericyte ghosts/loss, increased number of acellular capillaries, capillary loop formation, reduced capillary density, and thickened capillary BM.

Obesity and dyslipidemia have been proposed to be as important an issue in DR progression as that of hyperglycemia.[39] The obese Ossabaw pigs in this study gained ~40% body weight following 10 weeks on the Western diet and showed a significant increase in plasma glucose, with hyperinsulinemia and insulin resistance. Due to the diet, increased blood levels of cholesterol, HDL, LDL, and triglyceride were seen, mimicking conditions of the hyperlipidemia-associated risk of developing DR in human adult patients.[40,41] Recent studies proposed DR symptoms to be seen faster in patients aged 30 to 40 years old at T2DM diagnosis, versus patients age >50 years old at diagnosis.[42,43] Evidence also showed increased presentation in adolescents and youths diagnosed <20 years of age. This was seen in the United States study by the SEARCH for Diabetes in Youth Study Group where they found that 9% of T2DM young adults below 20 years of age presented with retinopathy.[37] In this group, patients had average diabetes duration of 8 years, and 72% were considered obese by the body mass index classification. They also reported a significant association between hyperglycemia, body mass index, and retinopathy. In another United States-based study, the TODAY study group conducted one of the largest adolescent T2DM studies[5] and found 13.7% of their 517 adolescents (ages 12–24 with 2–8 years of diabetes) manifested retinopathy.[6] All of the young patients had mild NPDR, and highest DR occurrence was reported in the 19 to 24 age bracket. Surprisingly, the TODAY group also found 5.3% retinopathy incidence in T2DM adolescents after only 2 to 4 years of diagnosis. The SEARCH report discussed this increased incidence of T2DM versus T1DM youths and postulated the more aggressive microvasculopathy progression in T2DM to be a result of difficulties in glycemic control in these young patients. Thus, preexisting conditions such as obesity and MetS at the young age[44] could elevate the risk of adolescents developing DR faster than their adult counterparts, highlighting the need to study the progression of DR in the young-onset of T2DM.

Retinal neural degeneration is documented to precede retinal microvasculopathy.[9] In the present study, we adopted high-resolution EM to characterize the extent of neuronal cell damage in the pig retina. The cross section of obese Ossabaw pig retinas did not show significant thinning of the retina. This was not surprising as retinal thinning in humans was reported in adult patients over 50 years old, with more than 10 years of diabetes.[45] Nevertheless, cellular derangement was seen in histologic examination of the Western diet-fed pigs. Ultrastruc-

Table. Capillary Density in Lean and Obese Ossabaw Pig Retinas

	Lean	Obese	*P*
Capillary density, capillary/mm^2	68 ± 25	31 ± 14	<0.01

Quantification of capillaries density presented as capillary count per mm^2 of retina cross section surface area. Data shown as mean ± SD.

Investigative Ophthalmology & Visual Science

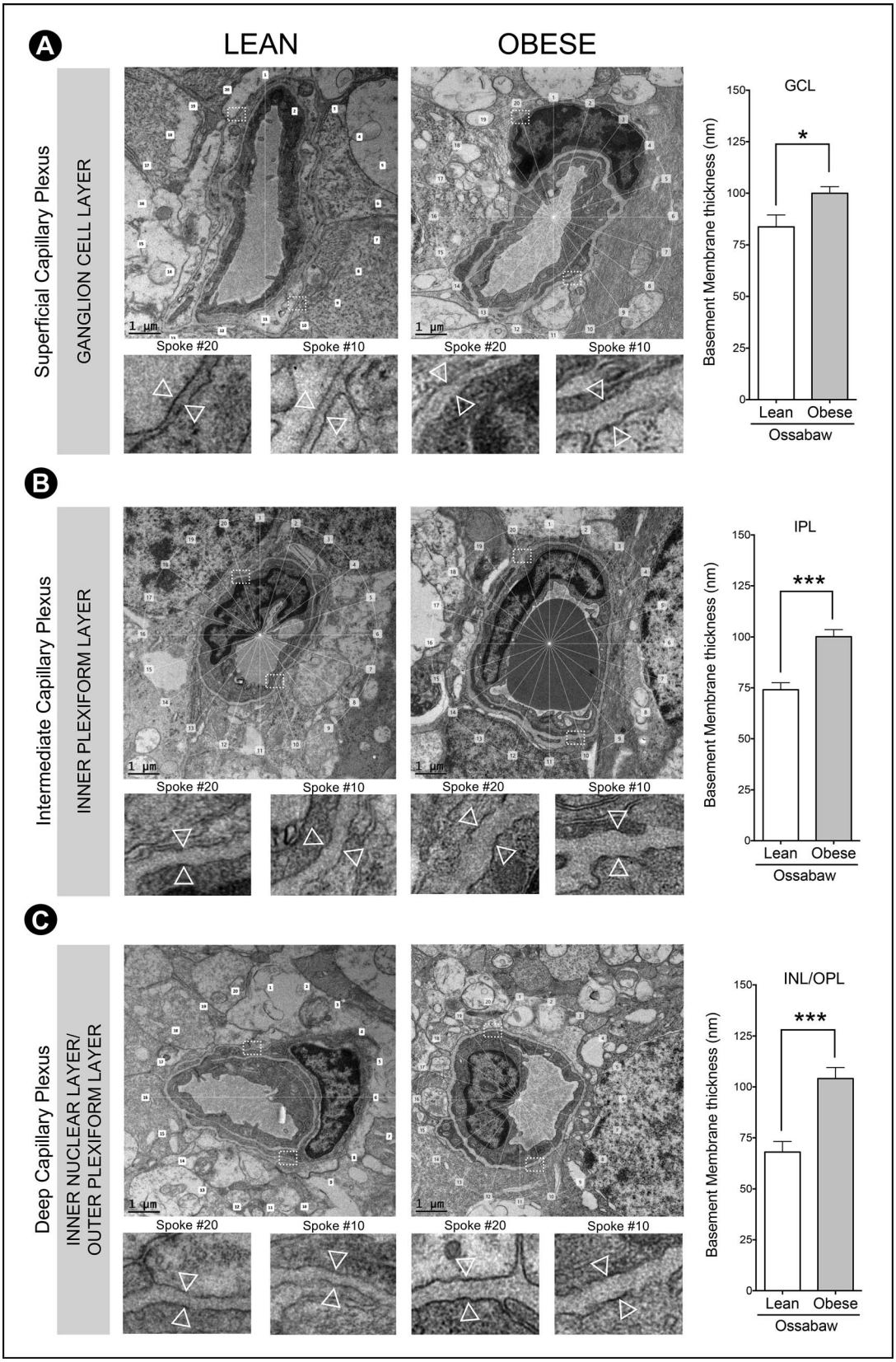

Figure 4. Increased BM thickness in Ossabaw pigs fed a Western diet. Representative EM images of retinal capillaries in the (**A**) superficial, (**B**) intermediate, and (**C**) deep capillary plexi, overlaid with a 20-spoke radial grid. Inset shows enlarged view of BM at spokes 20 and 10 for each image. BM was measured using ImageJ, by drawing a straight line perpendicular to the boundaries of the BM (denoted by *arrowhead*). Width measurements were averaged for the comparison between the lean and obese groups, which showed the BM to be consistently thicker across capillary plexi in the GCL, IPL, and INL/OPL of the obese Ossabaw pigs. $n = 3$ eyes per group; $n \geq 10$ capillaries per eye. $^{*}P < 0.05$ and $^{***}P < 0.001$. *Scale bar*: 1 µm.

Investigative Ophthalmology & Visual Science

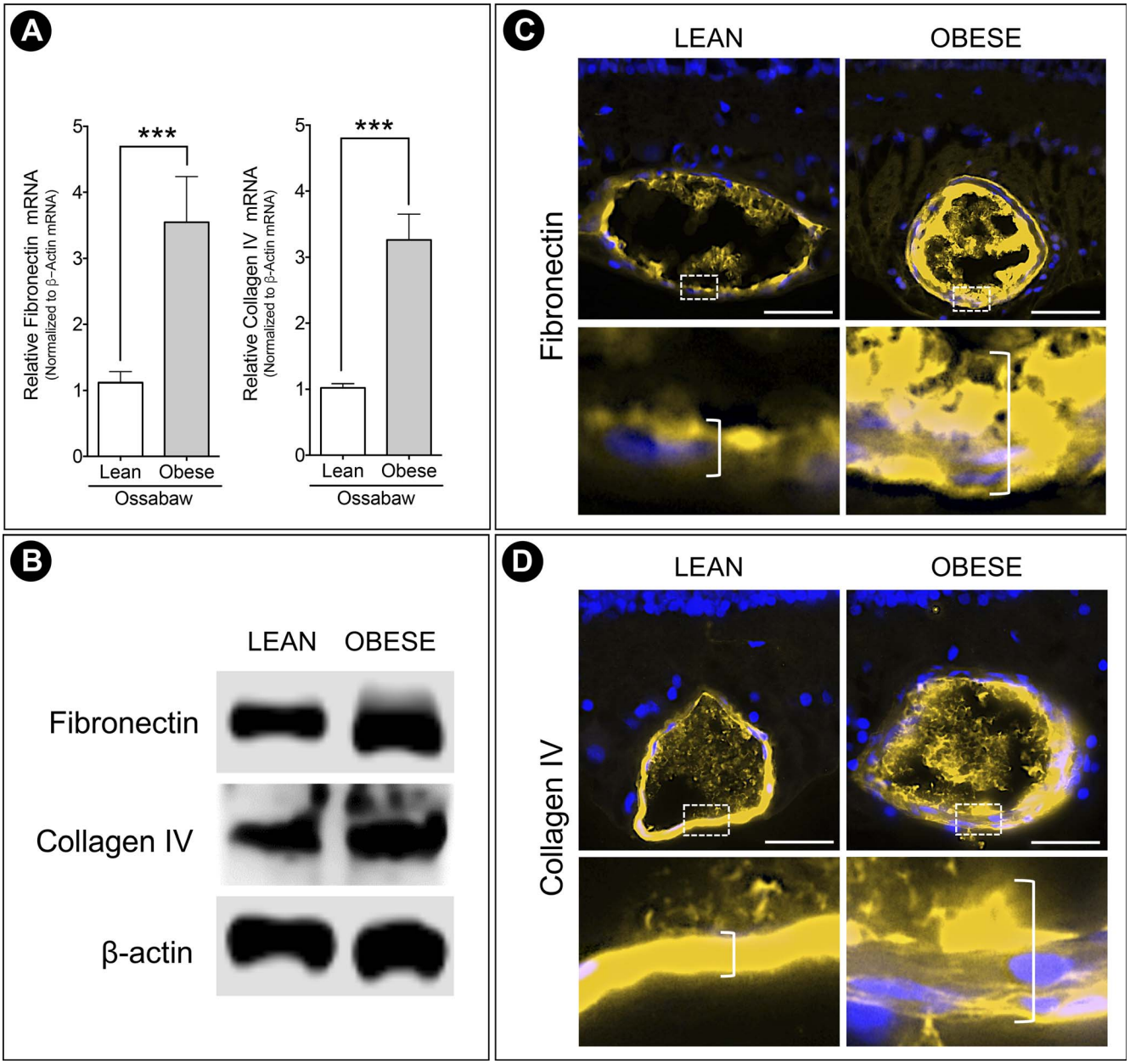

Figure 5. Elevated production of BM components in obese pigs. (**A**) Real-time PCR showed upregulation of fibronectin and collagen IV transcripts in the Western diet-fed pigs, which was supported by (**B**) Western blot protein expression. Representative immunohistochemistry staining images of (**C**) fibronectin and (**D**) collagen IV further showed elevated production of BM proteins in the obese Ossabaw pig retinal capillaries. Insets highlight increased capillary wall thickness (denoted by *open bracket*) in obese animals compared to lean controls. $n = 3$ eyes per group. $^{***}P < 0.001$. *Scale bar*: 50 μm.

tural examination showed multiple lesions throughout their retina, with cellular inclusions and hypervacuolations in the GCL and INL. Similar observations have been made earlier in T1DM and T2DM rodent models.[46,47] Axonal swelling was seen in the pig nerve fiber layer, which corresponds to the previous observations made in rodent diabetic retina.[48] The outer retina in the obese Ossabaw pigs was also found to be altered, with swelling of the PhR-inner segments, disorganization of outer segments and disruption of discs. Likewise, similar observations were made in streptozocin-treated T1DM rats.[49] FJC stain further supported these degenerative changes, with increased staining throughout the obese retina as compared to lean controls, in several layers of the retina. However, further studies are required to decipher the mechanisms involved in the neuronal loss.

Early vascular changes in DR are characterized by the loss of pericytes, thickening of the BM, and formation of the acellular capillary.[13] In this study, the Ossabaw pigs showed enhanced microvascular damage, evident by the decreased total pericyte numbers, significantly reduced pericyte to endothelial ratio, and increased acellular capillaries formation per millimeter length of the microvessel. Hyperglycemia appears to switch endothelial cells from quiescent to a proinflammatory and proangiogenic state,[50] which induces the production of BM components, leading to thickening of the underlying basal lamina.[51] Young obese Ossabaw pigs showed an increased production of fibronectin and collagen IV at the transcript and

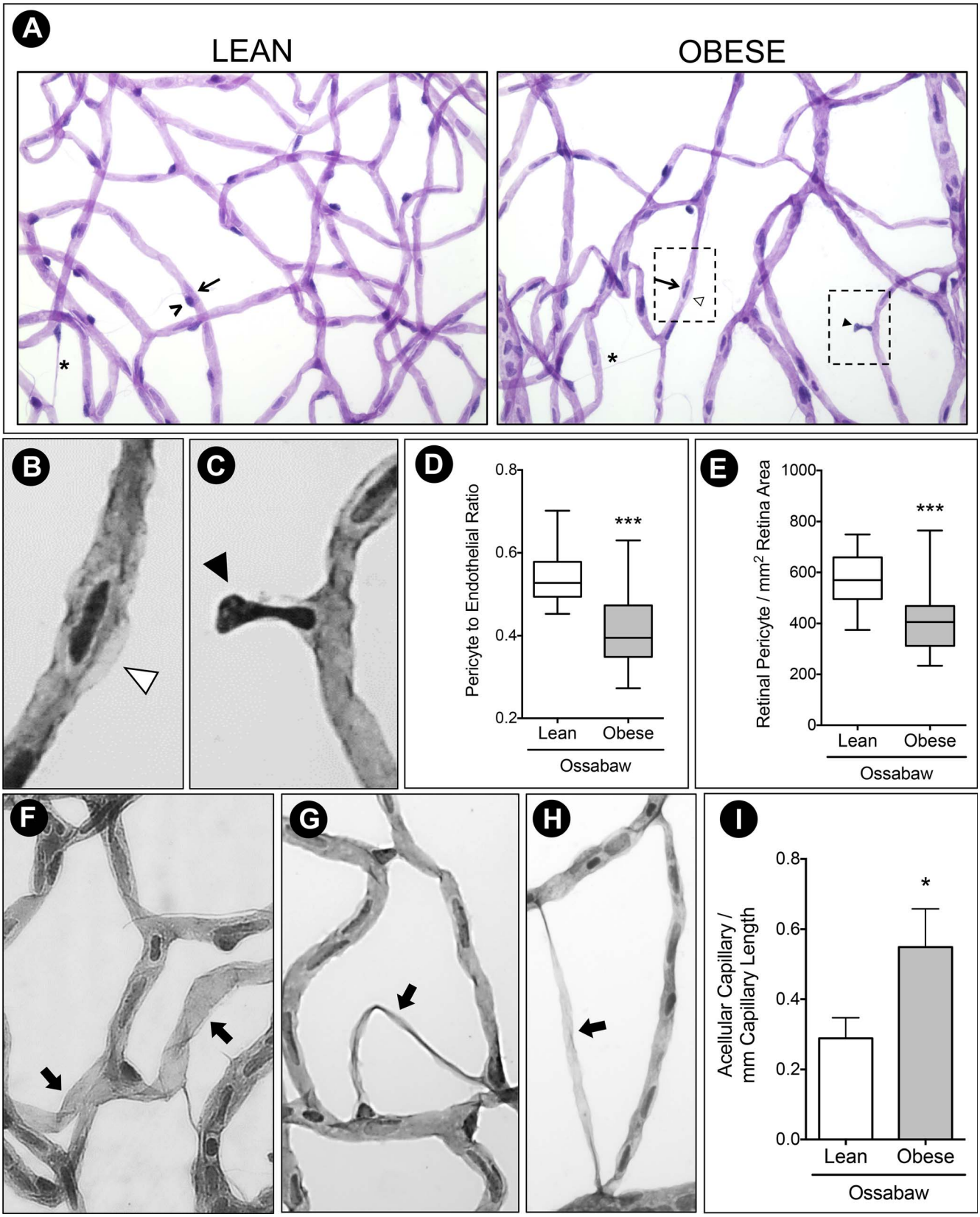

Figure 6. Pericyte ghost and acellular capillaries in Western diet-fed Ossabaw pigs. (**A**) Trypsin digest of Ossabaw pig retinas revealed uneven capillary caliber in the obese group, with pericyte lost (*black arrowhead*) and pericyte ghost (*white arrowhead*). Migrating pericytes (*asterisk*) can be seen in both animal groups. (**B**) Inset of pericyte ghost. (**C**) Inset of pericyte dropout. (**D**) Pericyte to endothelial ratio was significantly reduced in obese pigs compared to the lean control, evident by (**E**) decreased total retinal pericyte count in obese Ossabaw pigs. (**F–H**) Representative images of acellular capillaries (*thick arrow*) identified and quantified in Ossabaw pig retinas. (**I**) Count of acellular capillaries showed 50% increase per millimeter capillary length in Western diet-fed pigs. ^, pericyte cell; arrow, endothelial cell. $n = 3$ eyes per group. $^{*}P < 0.05$ and $^{***}P < 0.001$.

Investigative Ophthalmology & Visual Science

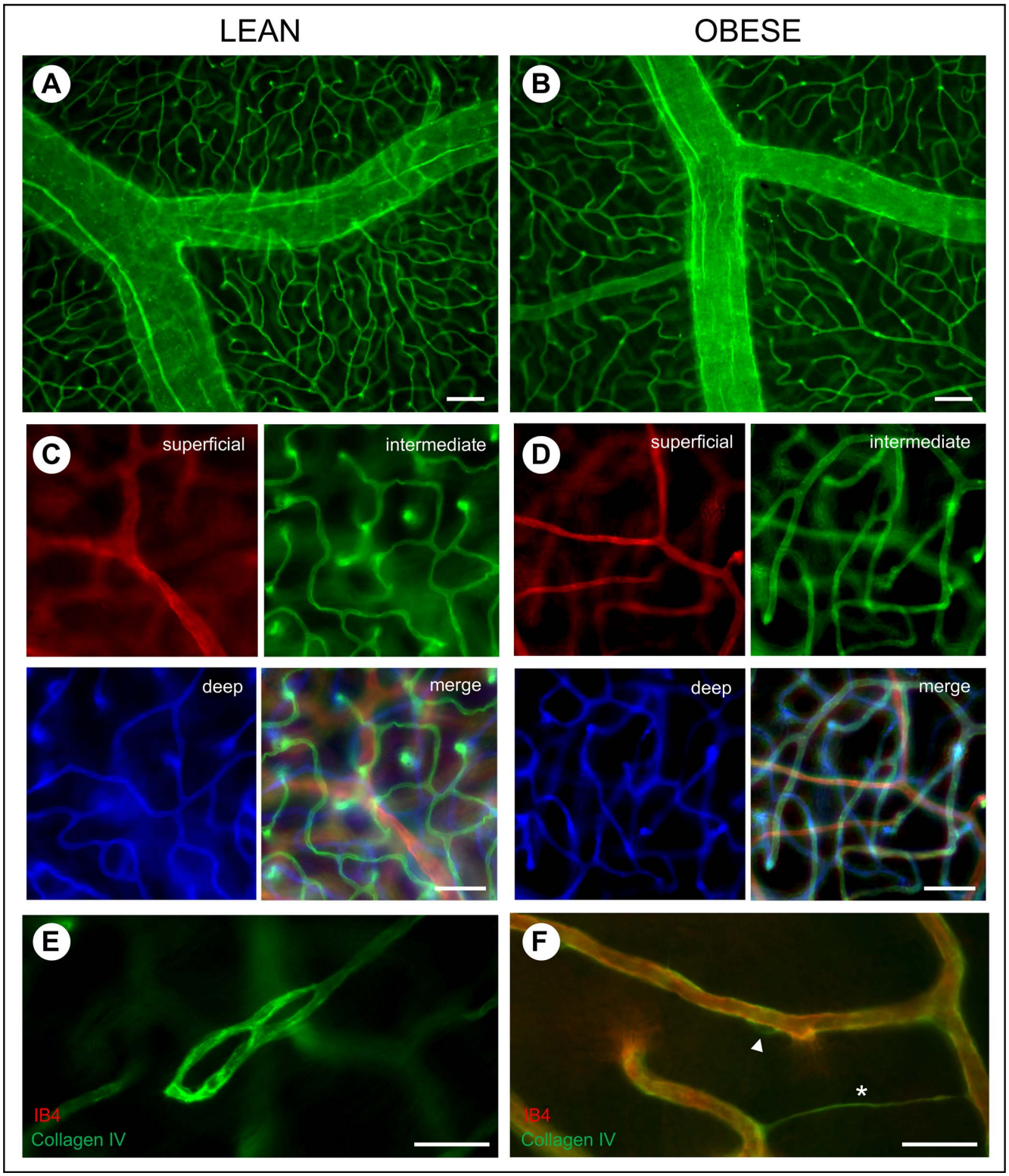

Figure 7. Arteriolar narrowing and reduced capillary density in Ossabaw mini pigs. Retina flatmount staining with Isolectin IB4 was used to visualize retinal vasculature. (**A**, **B**) Representative image of arteriole in similar regions of lean and obese pigs showed a slight reduction in vessel caliber after Western diet. Capillary density was also reduced in obese animals. (**C**, **D**) Composite and individual images of superficial, intermediate, and deep capillary plexi showed disruption in the intermediate capillary network of the obese Ossabaw pigs. (**E**) A representative example of terminal capillary tubes seen in Western diet-fed pigs. (**F**) Double immunostaining on retinal flatmount using collagen IV and isolectin IB4 shows pericyte ghost (*arrowhead*) and acellular capillary (*asterisk*) in the obese Ossabaw pigs. $n = 3$ eyes per group. *Scale bar*: 25 μm.

Investigative Ophthalmology & Visual Science

protein levels, which led to the increase in their microvascular BM width after only 10 weeks of the Western diet. This phenomenon was much faster than previous reports of chemically-induced T1DM in Yucatan[52] and Yorkshire[53] pigs. In these studies, Yucatan pigs were induced at 9 to 12 months of age for a diabetes duration of 4 months, whereas Yorkshire pigs were induced for a diabetes duration of 4 to 8 months. Hence, this reiterates the propensity for DR progression in young-onset diabetes to be much more aggressive than adult-onset diabetes. Reduced capillary density and arteriolar caliber were also observed in the Ossabaw pigs following Western diet-induced hyperlipidemia. Retinal vessel density had been reported to significantly reduce in mild DR patients with a diabetes duration of >10 years.[54] Also, capillary rarefaction had been seen in patients with less than 10 years of T2DM diagnosis.[55] However, there is no literature available on capillary density in adolescent DR patients. In contrast, dyslipidemia and retinal vascular caliber have been demonstrated to be significantly related in adolescents aged 12 to 17 years.[56] Specifically, increased total cholesterol, triglyceride, and LDL cholesterol were associated with retinal arteriolar narrowing. Interestingly, arteriolar narrowing was not observed in children less than 12 years old,[56] indicating the adverse impact of childhood dyslipidemia on the microvascular system in young ages.

Large animal models for DR are particularly valuable for their translational potential due to their pathophysiologic similarity to human conditions. The pig and human retinas have long been characterized and described to be similar in size, topography, and vasculature.[57] Not surprisingly, retinal research in pigs is scarce due to the lack of molecular reagents and antibodies[14] and the high cost of maintenance and genetic modifications. Studies of T2DM in pig models often use the Yucatan, Gottingen, and Yorkshire strains,[58] of which only the Yucatan[52] and Yorkshire pigs[53] were studied for retinal changes. Although Yucatan pigs fed an atherogenic diet are also models for MetS, a comparison between Ossabaw and Yucatan pigs showed the former to be a superior model of MetS,[25] and in our study, a better model for DR presentation. Nevertheless, the lack of retinal imaging and functional data remains a limitation, as we were unable to perform it because this study was part of a multiorgan, large pig study of the National Swine Research Center, University of Missouri, Columbia.[22]

In conclusion, Western diet-fed Ossabaw pigs exhibited retinal neurodegenerative and microvascular changes at a young age. This could be attributed to early-onset dyslipidemia and hyperglycemia, in addition to their inherent aggravated propensity for obesity and MetS, leading to exacerbated progression of DR. Hence, this study presents characteristics of DR in the young adults, indicating the Ossabaw pig to be a potential model for studying DR in T2DM.

Acknowledgements

The authors thank Tommi White from the University of Missouri, Electron Microscopy Core Facility (EMC) for her expert consult. The authors acknowledge a startup fund from Veterinary Medicine and Surgery, University of Missouri, Columbia, MO to SSC.

Supported by National Institutes of Health Grants U42-531 ODO011140 and NIH K01 HL-124403 (JP) and American Heart postdoctoral fellowship number 16POST2776005 (TDO). The authors alone are responsible for the writing and content of the paper.

Disclosure: **R.R. Lim**, None; **D.G. Grant**, None; **T.D. Olver**, None; **J. Padilla**, None; **A.M. Czajkowski**, None; **T.R. Schnurbusch**, None; **R.R. Mohan**, None; **D.P. Hainsworth**, None; **E.M. Walters**, None; **S.S. Chaurasia**, None

References

1. International Diabetes Federation. *IDF Diabetes Atlas*. 8th ed. Brussels, Belgium: International Diabetes Federation, 2017. Available at: http://www.diabetesatlas.org.
2. Viner R, White B, Christie, D. Type 2 diabetes in adolescents: a severe phenotype posing major clinical challenges and public health burden. *Lancet*. 2017;389:2252–2260.
3. Lobstein T, Jackson-Leach R. Planning for the worst: estimates of obesity and comorbidities in school-age children in 2025. *Pediatr Obes*. 2016;11:321–325.
4. Ogden CL, Carroll MD, Lawman HG, et al. Trends in obesity prevalence among children and adolescents in the United States, 1988-1994 through 2013-2014. *JAMA*. 2016;315:2292–2299.
5. Copeland KC, Zeitler P, Geffner M, et al. Characteristics of adolescents and youth with recent-onset type 2 diabetes: the TODAY cohort at baseline. *J Clin Endocrinol Metab*. 2011;96:159–167.
6. TODAY Study Group. Retinopathy in youth with type 2 diabetes participating in the TODAY clinical trial. *Diabetes Care*. 2013;36:1772–1774.
7. Booth FW, Roberts CK, Laye MJ. Lack of exercise is a major cause of chronic diseases. *Compr Physiol*. 2012;2:1143–1211.
8. Cheung N, Mitchell P, Wong TY. Diabetic retinopathy. *Lancet*. 2010;376:124–136.
9. Lynch SK, Abràmoff MD. Diabetic retinopathy is a neurodegenerative disorder. *Vision Res*. 2017;139:101–107.
10. Lecleire-Collet A, Audo I, Aout M, et al. Evaluation of retinal function and flicker light-induced retinal vascular response in normotensive patients with diabetes without retinopathy. *Invest Ophthalmol Vis Sci*. 2011;52:2861–2867.
11. Tyrberg M, Lindblad U, Melander A, Lövestam-Adrian M, Ponjavic V, Andréasson S. Electrophysiological studies in newly onset type 2 diabetes without visible vascular retinopathy. *Doc Ophthalmol*. 2011;123:193–198.
12. Cogan DG, Toussaint D, Kuwabara T. Retinal vascular patterns. IV. Diabetic retinopathy. *Arch Ophthalmol*. 1961;66:366–378.
13. Curtis TM, Gardiner TA, Stitt AW. Microvascular lesions of diabetic retinopathy: clues toward understanding pathogenesis? *Eye* (*Lond*). 2009;23:1496–1508.
14. Robinson R, Barathi VA, Chaurasia SS, Wong TY, Kern TS. Update on animal models of diabetic retinopathy: from molecular approaches to mice and higher mammals. *Dis Model Mech*. 2012;5:444–456.
15. Wang B, Chandrasekera PC, Pippin JJ. Leptin- and leptin receptor-deficient rodent models: relevance for human type 2 diabetes. *Curr Diabetes Rev*. 2014;10:131–145.
16. King AJ. The use of animal models in diabetes research. *Br J Pharmacol*. 2012;166:877–894.
17. Lai AK, Lo AC. Animal models of diabetic retinopathy: summary and comparison. *J Diabetes Res*. 2013;2013:106594.
18. Sturek M, Alloosh M, Wenzel J, et al. Ossabaw Island miniature swine: cardiometabolic syndrome assessment. In: Swindle MM, ed. *Swine in the Laboratory: Surgery, Anesthesia, Imaging, and Experimental Techniques*. 2nd ed. Boca Raton: CRC Press; 2007:397–402.
19. Dyson M, Alloosh M, Vuchetich J, Mokelke E, Sturek M. Components of metabolic syndrome and coronary artery disease in female Ossabaw swine fed excess atherogenic diet. *Comp Med*. 2006;56:35–45.
20. Alberti KG, Eckel RH, Grundy SM, et al. Harmonizing the metabolic syndrome: a joint interim statement of the International Diabetes Federation Task Force on Epidemiology and Prevention; National Heart, Lung, and Blood Institute;

American Heart Association; World Heart Federation; International Atherosclerosis Society; and International Association for the Study of Obesity. *Circulation*. 2009;120:1640–1645.

21. Olijhoek JK, van der Graaf Y, Banga JD, et al. The metabolic syndrome is associated with advanced vascular damage in patients with coronary heart disease, stroke, peripheral arterial disease or abdominal aortic aneurysm. *Eur Heart J*. 2004;25:342–348.
22. Olver TD, Grunewald ZI, Jurrissen TJ, et al. Microvascular insulin resistance in skeletal muscle and brain occurs early in the development of juvenile obesity in pigs. *Am J Physiol Regul Integr Comp Physiol*. 2018;314:R252–R264.
23. Bender SB, Tune JD, Borbouse L, Long X, Sturek M, Laughlin MH. Altered mechanism of adenosine-induced coronary arteriolar dilation in early-stage metabolic syndrome. *Exp Biol Med* (*Maywood*). 2009;234:683–692.
24. Panasevich MR, Meers GM, Linden MA, et al. High fat, high fructose, high cholesterol feeding causes severe NASH and cecal microbiota dysbiosis in juvenile Ossabaw swine. *Am J Physiol Endocrinol Metab*. 2018;314:E78–E92.
25. Neeb ZP, Edwards JM, Alloosh MA, Long X, Mokelke EA, Sturek M. Metabolic syndrome and coronary artery disease in Ossabaw compared to Yucatan swine. *Comp Med*. 2010;60:300–315.
26. Li Z, Woollard JR, Wang S, et al. Increased glomerular filtration rate in early metabolic syndrome is associated with renal adiposity and microvascular proliferation. *Am J Physiol Renal Physiol*. 2011;301:F1078–1087.
27. Siperstein MD, Unger RH, Madison LL. Studies of muscle capillary basement membranes in normal subjects, diabetic, and prediabetic patients. *J Clin Invest*. 1968;47:1973–1999.
28. Kern TS, Engerman RL. Capillary lesions develop in retina rather than cerebral cortex in diabetes and experimental galactosemia. *Arch Ophthalmol*. 1996;114:306–310.
29. Chronopoulos A, Roy S, Beglova E, Mansfield K, Wachtman L, Roy S. Hyperhexosemia-induced retinal vascular pathology in a novel primate model of diabetic retinopathy. *Diabetes*. 2015;64:2603–2608.
30. Boeri D, Cagliero E, Podestá F, Lorenzi M. Vascular wall von Willebrand factor in human diabetic retinopathy. *Invest Ophthalmol Vis Sci*. 1994;35:600–607.
31. Beauchemin ML. The fine structure of the pig's retina. *Albrecht Von Graefes Arch Klin Exp Ophthalmol*. 1974;190:27–45.
32. Chidlow G, Wood JP, Sarvestani G, Manavis J, Casson RJ. Evaluation of Fluoro-Jade C as a marker of degenerating neurons in the rat retina and optic nerve. *Exp Eye Res*. 2009;88:426–437.
33. Zeitler P, Fu J, Tandon N, et al. ISPAD Clinical practice consensus guidelines 2014. Type 2 diabetes in the child and adolescent. *Pediatr Diabetes*. 2014;15:26–46.
34. McNally PG, Raymond NT, Swift PG, Hearnshaw JR, Burden AC. Does the prepubertal duration of diabetes influence the onset of microvascular complications? *Diabet Med*. 1993;10:906–908.
35. Cho YH, Craig ME, Donaghue KC. Puberty as an accelerator for diabetes complications. *Pediatr Diabetes*. 2014;15:18–26.
36. Reiland S. Growth and skeletal development of the pig. *Acta Radiol Suppl*. 1978;358:15–22.
37. Dabelea D, Stafford JM, Mayer-Davis EJ, et al. Association of type 1 diabetes vs. type 2 diabetes diagnosed during childhood and adolescence with complications during teenage years and young adulthood. *JAMA*. 2017;317:825–835.
38. Wang SY, Andrews CA, Herman WH, Gardner TW, Stein JD. Incidence and risk factors for developing diabetic retinopathy among youths with type 1 or type 2 diabetes throughout the United States. *Ophthalmology*. 2017;124:424–430.
39. Hammer SS, Busik JV. The role of dyslipidemia in diabetic retinopathy. *Vision Res*. 2017;139:228–236.
40. Larsson LI, Alm A, Lithner F, Dahlén G, Bergström R. The association of hyperlipidemia with retinopathy in diabetic patients aged 15-50 years in the county of Umeå. *Acta Ophthalmol Scand*. 1999;77:585–591.
41. Zhang HY, Wang JY, Ying GS, Shen LP, Zhang Z. Serum lipids and other risk factors for diabetic retinopathy in Chinese type 2 diabetic patients. *J Zhejiang Univ Sci B*. 2013;14:392–399.
42. Song SH. Significant retinopathy in young-onset type 2 vs. type 1 diabetes: a clinical observation. *Int J Clin Pract*. 2016;70:853–860.
43. Li L, Ji L, Guo X, Ji Q, Gu W, Zhi X, et al. Prevalence of microvascular diseases among tertiary care Chinese with early versus late onset of type 2 diabetes. *J Diabetes Complications*. 2015;29:32–37.
44. Weinstock RS, Drews KL, Caprio S, Leibel NI, McKay SV, Zeitler PS; TODAY Study Group. Metabolic syndrome is common and persistent in youth-onset type 2 diabetes: Results from the TODAY clinical trial. *Obesity* (*Silver Spring*). 2015;23:1357–1361.
45. Van Dijk HW, Verbraak FD, Kok PH, et al. Early neurodegeneration in the retina of type 2 diabetic patients. *Invest Opthalmol Vis Sci*. 2012;53:2715–2719.
46. Bogdanov P, Corraliza L, Villena JA, et al. The db/db mouse: a useful model for the study of diabetic retinal neurodegeneration. *PLoS One*. 2014;9:e97302.
47. Wang H, Zheng Z, Gong Y, Zhu B, Xu X. U83836E inhibits retinal neurodegeneration in early-stage streptozotocin-induced diabetic rats. *Ophthalmic Res*. 2011;46:19–24.
48. Abcouwer SF, Gardner TW. Diabetic retinopathy: loss of neuroretinal adaptation to the diabetic metabolic environment. *Ann N Y Acad Sci*. 2014;1311:174–190.
49. Énzsöly A, Szabó A, Kántor O, et al. Pathologic alterations of the outer retina in streptozotocin-induced diabetes. *Invest Opthalmol Vis Sci*. 2014;55:3686–3699.
50. Popov D. Endothelial cell dysfunction in hyperglycemia: phenotypic change, intracellular signaling modification, ultrastructural alteration, and potential clinical outcomes. *Int J Diabetes Mellit*. 2010:2:189–195.
51. Roy S, Ha J, Trudeau K, Beglova E. Vascular basement membrane thickening in diabetic retinopathy. *Curr Eye Res*. 2010;35:1045–1056.
52. Hainsworth DP, Katz ML, Sanders DA, Sanders DN, Wright EJ, Sturek M. Retinal capillary basement membrane thickening in a porcine model of diabetes mellitus. *Comp Med*. 2002;52:523–529.
53. Lee SE, Ma W, Rattigan EM, et al. Ultrastructural features of retinal capillary basement membrane thickening in diabetic swine. *Ultrastruct Pathol*. 2010;34:35–41.
54. Kim AY, Chu Z, Shahidzadeh A, Wang RK, Puliafito CA, Kashani AH. Quantifying microvascular density and morphology in diabetic retinopathy using spectral-domain optical coherence tomography angiography. *Invest Ophthalmol Vis Sci*. 2016;57:OCT362–OCT370.
55. Jumar A, Harazny JM, Ott C, et al. Retinal capillary rarefaction in patients with type 2 diabetes mellitus. *PLoS One*. 2016;11:e0162608.
56. Xiao W, Guo X, Ding X, He M. Serum lipid profiles and dyslipidemia are associated with retinal microvascular changes in children and adolescents. *Sci Rep*. 2017;7:44874.
57. Swindle MM, Smith AC. Swine in biomedical research. In: Conn PM, ed. *Sourcebook of Models for Biomedical Research*. New Jersey: Humana Press Inc.; 2008:233–239.
58. Bellinger DA, Merricks EP, Nichols TC. Swine models of type 2 diabetes mellitus: insulin resistance, glucose tolerance, and cardiovascular complications. *ILAR J*. 2006;47:243–258.

Investigative Ophthalmology & Visual Science